European Journal of Medicinal Chemistry 226 (2021) 113814

Contents lists available at ScienceDirect

European Journal of Medicinal Chemistry

journal homepage: http://www.elsevier.com/locate/ejmech

Indomethacin-based PROTACs as pan-coronavirus antiviral agents

Jenny Desantis [a, 1], Beatrice Mercorelli [a, 1], Marta Celegato [a], Federico Croci [b], Alessandro Bazzacco [a], Massimo Baroni [c], Lydia Siragusa [d], Gabriele Cruciani [b], Arianna Loregian [a, **, 2], Laura Goracci [b, *, 2]

[a] Department of Molecular Medicine, University of Padua, Padua, Italy
[b] Department of Chemistry, Biology, and Biotechnology, University of Perugia, Italy
[c] Molecular Discovery Ltd., Centennial Park, Borehamwood, Hertfordshire, United Kingdom
[d] Molecular Horizon Srl, Bettona, 06084, Italy

ARTICLE INFO

Article history:
Received 26 May 2021
Received in revised form
26 August 2021
Accepted 28 August 2021
Available online 4 September 2021

Keywords:
PROTAC
Coronavirus
SARS-CoV-2
Indomethacin
Antiviral agents
PGES-2

ABSTRACT

Indomethacin (INM), a well-known non-steroidal anti-inflammatory drug, has recently gained attention for its antiviral activity demonstrated in drug repurposing studies against severe acute respiratory syndrome coronavirus-2 (SARS-CoV-2). Although the mechanism of action of INM is not yet fully understood, recent studies have indicated that it acts at an early stage of the coronaviruses (CoVs) replication cycle. In addition, a proteomic study reported that the anti-SARS-CoV-2 activity of INM could be also ascribed to its ability to inhibit human prostaglandin E synthase type 2 (PGES-2), a host protein which interacts with the SARS-CoV-2 NSP7 protein. Although INM does not potently inhibit SARS-CoV-2 replication in infected Vero E6 cells, here we have explored for the first time the application of the Proteolysis Targeting Chimeras (PROTACs) technology in order to develop more potent INM-derived PROTACs with anti-CoV activity. In this study, we report the design, synthesis, and biological evaluation of a series of INM-based PROTACs endowed with antiviral activity against a panel of human CoVs, including different SARS-CoV-2 strains. Two PROTACs showed a strong improvement in antiviral potency compared to INM. Molecular modelling studies support human PGES-2 as a potential target of INM-based antiviral PROTACs, thus paving the way toward the development of host-directed anti-CoVs strategies. To the best of our knowledge, these PROTACs represent the first-in-class INM-based PROTACs with antiviral activity and also the first example of the application of PROTACs to develop pan-coronavirus agents.

1. Introduction

Since its identification in patients with severe pneumonia in Wuhan city, Hubei [1,2] the 2019 novel severe acute respiratory syndrome coronavirus 2 (SARS-CoV-2) has rapidly spread around the world causing the large-scale COVID-19 pandemic. As of 21 May 2021, SARS-CoV-2 infection has caused more than 165 million of confirmed positive cases, many hospitalizations, and more than 3.4 million deaths [3].

SARS-CoV-2 is an enveloped, positive-sense, single-stranded RNA virus characterized by the largest viral RNA genome found to date [4–6]. It belongs to the *Coronavirinae* subfamily (*Coronaviridae* family), which comprises four genera, i.e., α-, β-, γ-, and δ-coronavirus. Among the coronaviruses known to infect humans, the β-coronavirus genus includes SARS-CoV and SARS-CoV-2, MERS-CoV, HCoV-OC43 and HCoV-HKU1, while HCoV-229E and HCoV-NL63 belong to the α-coronavirus genus [7].

Currently, no specific antiviral drugs have been approved against SARS-CoV-2 and other human pathogenic coronaviruses, with the exception of remdesivir, which obtained an emergency use authorization in May 2020 for the treatment of patients with severe COVID-19 symptoms [8,9], but later in October 2020 WHO issued a recommendation against the use of remdesivir, given the controversial benefits in COVID-19 patients [10].

* Corresponding author.
** Corresponding author.
E-mail addresses: arianna.loregian@unipd.it (A. Loregian), laura.goracci@unipg.it (L. Goracci).
[1] co-first authors.
[2] co-last authors.

https://doi.org/10.1016/j.ejmech.2021.113814
0223-5234/

Given the severity of the SARS-CoV-2 outbreak, an intensive research effort from pharma companies, academic research labs, and other organizations is globally ongoing with the aim of identifying specific anti-coronavirus drugs [11–14].

Until now, drug repurposing represents one of the most pursued strategies elected so far by the scientific community to identify effective drugs for combating the COVID-19 pandemic. Indeed, this strategy can rapidly lead to the identification of existing clinically approved drugs able to prevent, control, or eradicate the SARS-CoV-2 infection, thus representing possible therapeutics for COVID-19 [13,15–17].

In this context, indomethacin (INM) (Fig. 1a), a non-steroidal anti-inflammatory drug (NSAID) with anti-inflammatory, analgesic, and antipyretic properties, has gained great attention from different research groups as potential treatment or adjunct for SARS-CoV-2/COVID-19 [18–21]. The pharmacological effect of INM as an NSAID drug is not yet fully understood, but it is commonly related to a potent and non-selective inhibition of the cyclo-oxygenase (COX)-1 and 2 enzymes, or prostaglandin G/H synthase [22,23]. However, INM is also known to inhibit phospholipase A2 (PLA-2) [24], and microsomal prostaglandin E synthase type 2 (mPGES-2) [23], all involved in eicosanoid biosynthesis. Concerning its antiviral effect against coronaviruses (CoVs), INM was previously shown to possess the ability to inhibit the replication of canine coronavirus (CCoV) and SARS-CoV [25,26]. In 2006, Amici et al. reported the *in vitro* activity of INM against human SARS-CoV (IC_{50} = 50 μM, Vero cells) and CCoV (IC_{50} = 5 μM, canine A72 cells) as well as *in vivo* antiviral efficacy in CCoV-infected dogs treated orally (1 mg/kg body weight) [26]. Recently, INM has been also investigated for its effect against SARS-CoV-2. Indeed, in April 2020, an open-label, single-arm, phase II clinical study was started to evaluate the efficacy and safety of oral INM in SARS-CoV-2 positive patients with mild COVID-19 symptoms (NCT04344457, n = 80) [27]. Moreover, by using an integrative, network-based deep-learning methodology, INM was reported by Zeng et al. as a possible repurposable drug candidate for COVID-19. This new therapeutic indication was validated by transcriptomic and proteomic data in SARS-CoV-2-infected human cells and data from ongoing clinical trials [20]. INM was also evaluated *in vitro* against SARS-CoV-2 alone or in combination with ketotifene [28]. Although in a 4-day cytopathic effect protection assay INM did not exhibit any antiviral activity (EC_{50} > 400 μM, Vero E6 cells), its evaluation in a virus yield reduction assay under reduced rounds of virus replication (48 h) showed an inhibition of SARS-CoV-2 replication with an EC_{50} of 100.1 μM (in infected Vero E6 cells) [28].

The mechanism of antiviral action of INM remains unknown, but different hypotheses have been postulated so far. In particular, results reported by Amici et al. indicate that INM does not affect virus infectivity, binding or entry into host cells, but acts at an early stage of coronaviruses replication cycle, causing a global repression of viral protein synthesis *via* a ds-RNA-dependent protein kinase R (PKR)-mediated pathway [26]. On the other hand, a recently published proteomic/chemoinformatic study on the SARS-CoV-2 interactome with human host proteins suggested that the anti-SARS-CoV-2 activity of INM could be ascribed to its ability to inhibit human prostaglandin E synthase type 2 (PGES-2, encoded by *PTGES2*) [21,29,30]. In fact, INM has been previously reported as PGES-2 inhibitor in the low nanomolar range [25,31] and PGES-2 has been found to interact with the SARS-CoV-2 NSP7 protein [21,29], which, along with NSP8, is a non-structural viral protein composing the viral primase complex that is part of the viral RNA polymerase machinery. Interestingly, PGES-2 resulted as a host proviral factor and the interaction between NSP7 and PGES-2 was found to be conserved across the three highly pathogenic CoVs SARS-CoV, SARS-CoV-2, and MERS-CoV [29,30], suggesting that PGES-2 may be a potential pan-CoV antiviral target, i.e., a target shared by all pathogenic CoVs that could be exploited for the development of universal anti-CoV strategies (from the Greek πᾶν, pan, meaning "involving all members" of a group).

Gordon and co-workers also found that COVID-19 patients treated with INM were less likely to require hospitalization than those treated with other anti-inflammatory drugs that do not target PGES-2, providing a connection between proteomics study and clinical data [29]. However, it is worth noting that the anti-SARS-CoV-2 potency of INM is limited in infected cells, being in the range of ~100 μM (this study and ref [28]). Taking this into account, we hypothesized that the exploitation of INM for PROTAC design could result in an enhancement of antiviral activity, since the degradation of the target PGES-2 could be obtained in addition to enzymatic inhibition and potentiate the antiviral effect.

In the past few years, PROteolysis TArgeting Chimeras (PROTACs) have become an exciting new paradigm to target proteins by promoting and achieving target proteins degradation *via* the ubiquitin-proteasome system (UPS) [32–37]. PROTACs are heterobifunctional molecules composed of a ligand for a protein of interest (POI) and an E3 ligase binder connected through a linker [38].

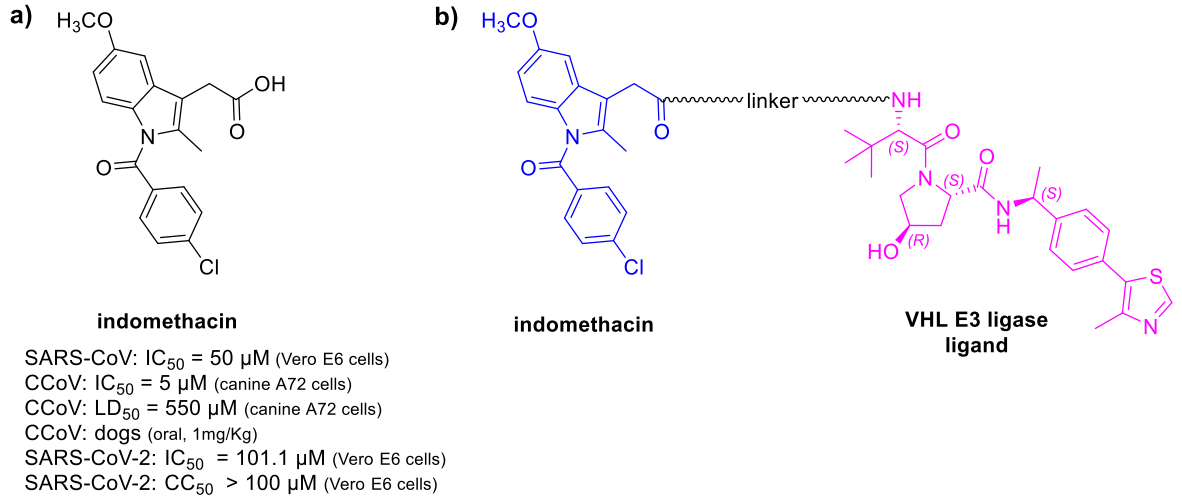

Fig. 1. **(a)** Chemical structure of INM. **(b)** General structure of the designed INM-based PROTACs. The IC_{50} value represents the compound concentration that inhibits 50% of viral replication. The CC_{50} value represents the compound concentration that inhibits 50% of cell viability.

They act by bringing the E3 ligase into close proximity of the POI, thus inducing its ubiquitination and subsequent UPS-dependent degradation [32,37]. Unlike traditional inhibitors, the removal of all the POI functions at once through POI degradation can achieve a more profound pharmacological effect than that obtained by only inhibiting a functional binding site [37]. Moreover, PROTACs do not require long-term and high-affinity binding to the POI, since a potent target degradation can be even obtained with modest-affinity POI ligands if a stable ternary complex is formed [37,39,40], thus permitting to reduce or even abrogate the development of drug resistance [32]. Despite the increasing interest in PROTAC technology, their application is still marginal in the field of antivirals, with only one well-characterized application reported against the hepatitis C virus NS3/4A protease [41]. The present study not only provided the proof-of-concept that targeted protein degradation may represent a valuable approach for antiviral design, but it also demonstrated that PROTACs are less prone to select viral mutants with impaired ligand binding and could thus be exploited in the case of viral resistance to conventional inhibitors [41]. So far, only one paper suggesting the possible use of PROTACs against SARS-CoV-2 has been published [42], but chemical structures were not disclosed.

In the present work, based on the experimental and clinical evidence accumulated to date, which suggests a potential therapeutic use of INM against SARS-CoV-2 infection, we decided to exploit INM to design PROTAC derivatives (Fig. 1) in order to investigate whether this emerging new technology could represent a valid approach also in the search for anti-coronavirus agents.

2. Result and discussion

2.1. Design and synthesis of INM-based PROTACs

Considering the INM carboxylic acid group as a suitable and easy site for linker attachment to exploit for amidation reaction, also due to the exposition of this group to the solvent (Figure S1), herein we designed and synthesized four INM-based PROTACs (2–5, Table 1) by conjugating INM with the Von Hippel Lindau (VHL) E3 ligase ligand *via* aliphatic and polyethylene glycol (PEG)ylated linkers.

In particular, INM (compound 1) was coupled by amidation reaction with the suitable VHL ligand properly functionalized with linkers in the presence of 1-[bis(dimethylamino)methylene]-1*H*-1,2,3-triazolo[4,5-*b*]pyridinium 3-oxid hexafluorophosphate (HATU) and *N*,*N*-diisopropylethylamine (DIPEA) at room temperature in dimethylformamide (DMF) (Scheme 1).

The VHL-linker intermediates 15–18 (Scheme 2) used for the synthesis of the final PROTACs were prepared starting from VHL ligand 6 [43] which was first coupled with the appropriate *N*-Boc protected amino acid linkers 7, 8, 9, and 10 through HATU-mediated amidation reaction and then finally deprotected to afford amino intermediates 15 [44], 16 [44], 17 [44], and 18.

2.2. Biological evaluation

The antiviral activity of the synthesized PROTAC compounds, along with INM, was first evaluated by plaque reduction assays (PRA) in Vero E6 cells infected with SARS-CoV-2/NL/2020 (Table 1). The viral RNA polymerase inhibitor remdesivir (RMV) was included as a positive control of inhibition [45]. As reported in Table 1, INM inhibited the replication of SARS-CoV-2 with an Effective Concentration (EC_{50}) of 94.9 μM, a value similar to those already reported for SARS-CoV and SARS-CoV-2 [26,28]. Among the four tested PROTACs, while the introduction of a short aliphatic as well as a PEGylated linker did not result in active PROTACs, compounds 3 (bearing a 6-methylene units linker) and 5 (bearing a piperazine-based linker) resulted the most potent compounds showing EC_{50} values of 18.1 μM and 21.5 μM, respectively. Indeed, as previously exemplified [39,40], despite INM showed only a weak antiviral activity (EC_{50} = 94.4 μM), INM-based PROTACs 3 and 5 demonstrated an almost 5-fold improved ability in inhibiting viral

Table 1
Antiviral activity and cytotoxicity of indomethacin and PROTAC compounds against SARS-CoV-2.

Compound	Linker	CC_{50}[a] (μM)	SARS-CoV-2/NL/2020 EC_{50}[b] (μM) (CI)[c]	SI[d]	SARS-CoV-2/Padova/2021 EC_{50} (μM) (CI)	SI
INM	_	>500	94.9 (53.3–175.2)	>5	N.D.	_
2	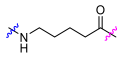	>200	>50	>4	>50	>4
3	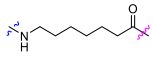	>200	18.1 (7.1–46.4)	>11	25.4 (9.8–69.2)	>8
4	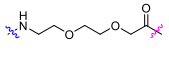	>200	>50	>4	>50	>4
5	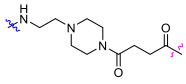	>250	21.5 (11.2–43.4)	>12	29.8 (14.5–41.9)	>8
RMV	_	373 ± 20	0.15 (0.11–0.20)	2487	0.25 (0.18–0.36)	1492

N.D., Not Determined.
[a] 50% Cytotoxic Concentration, the compound concentration that inhibits 50% of cell viability, as determined by MTT assay in Vero E6 cells at 72 h.
[b] Effective Concentration, the compound concentration that inhibits 50% of plaque formation, as determined by PRAs against different SARS-CoV-2 strains in Vero E6. Reported values represent data derived from n = 3 independent experiments in duplicate.
[c] CI, Confidence Interval, 95% Profile likelihood, calculated with GraphPad Prism 8.0 software.
[d] Selectivity Index, determined as the ratio between CC_{50}/EC_{50}.

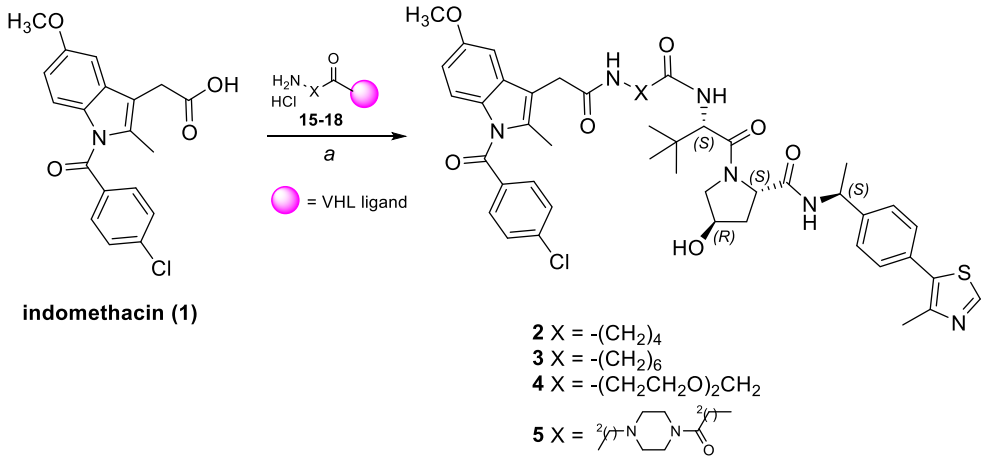

Scheme 1. *Reagents and conditions*: a) HATU, DIPEA, dry DMF, rt, 16 h.

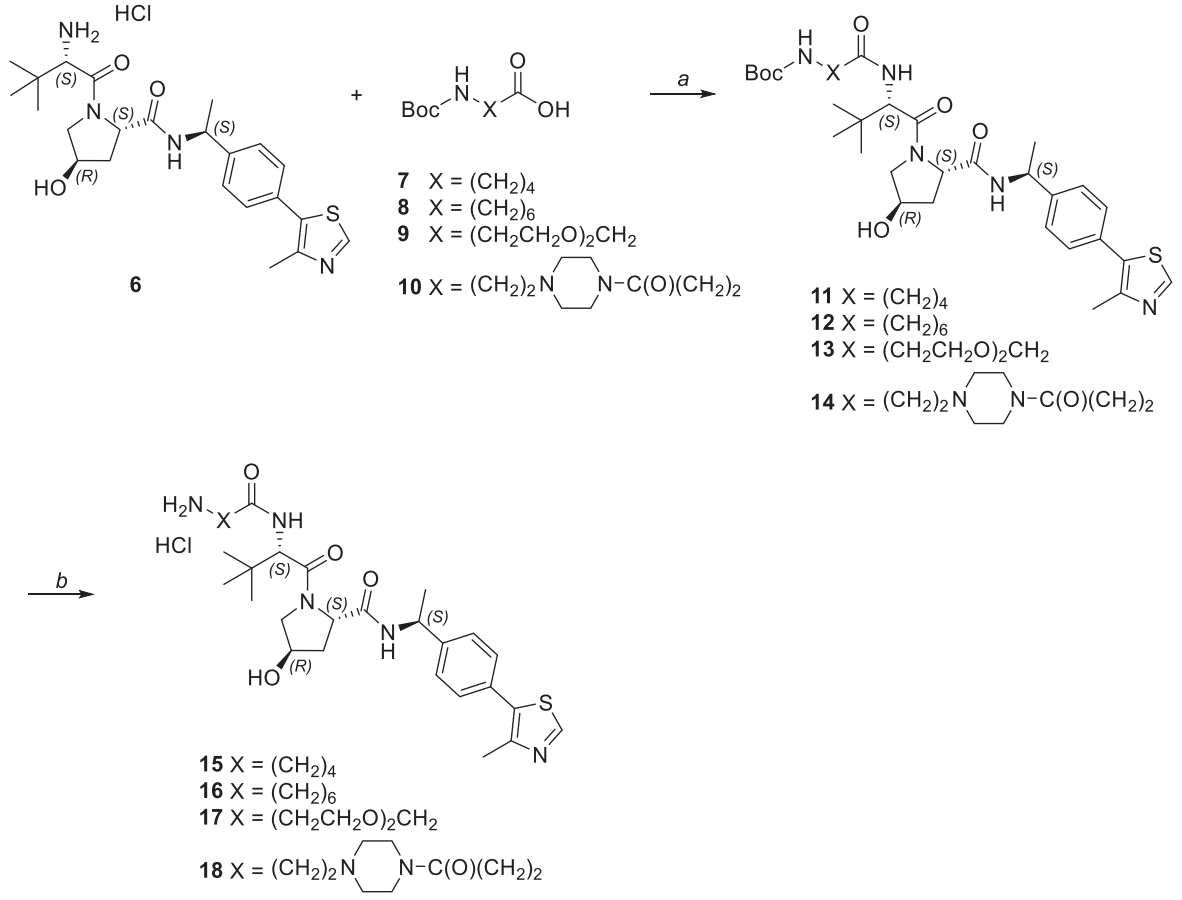

Scheme 2. *Reagents and conditions*: a) HATU, DIPEA, dry DMF, rt, 1–18 h; b) HCl 4 N in dioxane, rt, 1–18h.

replication. Their antiviral activity was also retained against a clinical SARS-CoV-2 isolate (SARS-CoV-2/Padova/2021, Table 1). In contrast, compounds 2 and 4 did not show dose-dependent inhibitory activity against any of the tested SARS-CoV-2 strains up to 50 μM (Table 1). To exclude that the observed antiviral activity could be due to toxic effects in the target cells, the cytotoxicity of the compounds was tested in parallel by MTT assays in Vero E6 cells. None of the compounds showed cytotoxicity up to a concentration of 200–250 μM (Table 1).

Interestingly, as reported in Table 2, both compound 3 and 5 not only inhibited SARS-CoV-2 replication, but they also showed antiviral activity against another β-coronavirus, i.e., HCoV-OC43 (EC_{50} = 4.7 and 2.5 μM, respectively). Moreover, we observed antiviral activity for 3 and 5 also against the α-coronavirus HCoV-229E, although compound 3 resulted less active against HCoV-229E compared to HCoV-OC43 (Table 2). Importantly, both compounds 3 and 5 did not show significant cytotoxicity also in MRC-5 cells, thus excluding that the possibility the antiviral activity of

Table 2
Antiviral activity and cytotoxicity of indomethacin-based PROTACs against human CoVs.

Compound	Linker	CC_{50}[a] (μM)	EC_{50}[b] (μM) (CI)[c]	
			HCoV-OC43	HCoV-229E
3	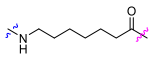	>250	4.7 (1.1–18.1)	36.5 (20.1–70.3)
5	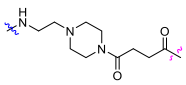	238 ± 17	2.5 (0.8–7.5)	3.2 (1.4–7.1)

[a] 50% Cytotoxic Concentration, the compound concentration that inhibits 50% of cell viability, as determined by MTT assay in MRC-5 cells at 72 h.
[b] Effective Concentration, the compound concentration that inhibits 50% of plaque formation, as determined by PRAs against different HCoV strains in MRC-5 cells. Reported values represent data derived from n = 3 independent experiments in duplicate.
[c] CI, Confidence Interval (95% Profile likelihood, calculated with GraphPad Prism 8.0 software).

these PROTAC derivatives of INM might be due to cytotoxic effects. Thus, both compounds 3 and 5 exhibited specific antiviral activity against pandemic and epidemic CoVs belonging to different genera of *Coronaviridae* family. To note, the fact that INM-derived PROTACs 3 and 5 resulted more active against HCoVs compared to SARS-CoV-2 could be ascribed to the different cell lines used in the experiments. In fact, for the HCoVs experiments, a human fibroblast cell line (MRC-5) was used and possible differences in E3 ligase VHL expression with respect to that in the simian Vero E6 cell line used for SARS-CoV-2 experiments could exist. Alternatively, also differences in the expression and/or activity of the PGES-2 target in the two cell lines cannot be excluded. Further studies will be aimed at investigating these aspects.

2.3. Molecular modelling studies

Although the limited number of compounds investigated in this study does not allow determination of a structure-activity relationship, which will be a topic for future studies, we were intrigued by the significant increased activity of compound 3 compared to 2, as they only differ by two methylene units. We hypothesized that the linker in compound 2 might be too short to allow the ternary complex formation and induce target degradation. Thus, a homology model of the human mPGES-2 was used to model the interaction of compounds 2 and 3 with the target and possibly explain the experimental data. An *in house* developed algorithm was used to explore the role of the length of the aliphatic linker in the ternary complex formation. Details on model building are provided in the experimental section. First, truncated structures of 2 and 3 missing the INM scaffold were built (Fig. 2-a,b), and VHL ligand moieties were superimposed onto the x-ray VHL ligand pose. Thus, the linker moiety was allowed to freely move and poses were inspected. Fig. 2-a,b clearly shows that the VHL ligand-protein interaction occurs in a very superficial region, and therefore both linkers are not buried but potentially available for complex generation. On the contrary, when the overall procedure was repeated by building the INM-linker moiety and removing the VHL ligand (Fig. 2-c,f), the linker in compound 2 resulted as buried into the target protein (the human mPGES-2 here as a homology model), and thus less prone to form the ternary complex. In the case of compound 3, the linker resulted as more able to expose its terminal group out of the target cavity, although by a limited amount. Compounds 4 and 5, whose linkers have a length that is comparable to the one in 3 despite the different chemical nature, resulted as able to form the ternary complex (data not shown).

Thus, we moved forward by building models of the potential PGES-2/Compound **3**/E3 and PGES-2/Compound **5**/E3 ternary complexes. Indeed, compounds **3** and **5** were found to be about 5-fold more active than INM suggesting that the formation of the ternary complex could take place and enhance the antiviral activity. An in house algorithm to predict PROTACs ternary complex formation was used (see Experimental section) and the best results are shown in Fig. 3-a,**b** and **e-f**. Our models showed a nice interlocking between the two proteins and with the ligand moieties of optimized **3** and **5**, having coordinates very similar to the ones of the ligands in the E3 ligase x-ray structure (PDB ID: 5T35) and in the human mPGES-2 homology model (see Experimental section) (Fig. 3-c,**d** and **g,h**) also after optimization of the overall complex.

A comparison between the proposed PGES-2/Compound **3**/E3 and PGES-2/Compound **5**/E3 ternary complexes suggested that **3** allows the two proteins to be closer than in the case of **5** (Fig. 3-a,b and **e,f** respectively), possibly due to the greater rigidity of the piperazine-containing linker in **5**. For clarity, Fig. 4 describes the poses of **3** and **5** at the joining region of the ternary complex. Concerning compound **3**, the aliphatic linker was stabilized by hydrophobic interactions, fitting the hydrophobic region defined by Y111 in VHL E3 ligase and F112, V243 and H244 in mPGES-2 (Fig. 4-a). This favorable hydrophobic interaction might explain why the PEGylated analogue **4** was not active in PRA. In addition, the packed conformation of **3** seemed to be stabilized by an intramolecular H-bond between a carbonyl group and a nitrogen of the amide function at the opposite edges of the linker. In the case of **5**, the linker including the piperazine moiety was localized in the same region, although the two proteins are more distant from each other. The piperazine ring is always localized close to a hydrophobic region, which is more concentrated at the protein-protein interface. In addition to hydrophobic interactions with the piperazine, in this model Y111 was oriented toward not the amide moiety anchoring the linker to the VHL ligand, possibly stabilizing it through a H-bond (Fig. 4-b).

3. Conclusions

PROTAC technology has been applied to a variety of targets and PROTACs have been recently suggested as possible next-generation anti-coronavirus drugs. Here, we present the first PROTAC

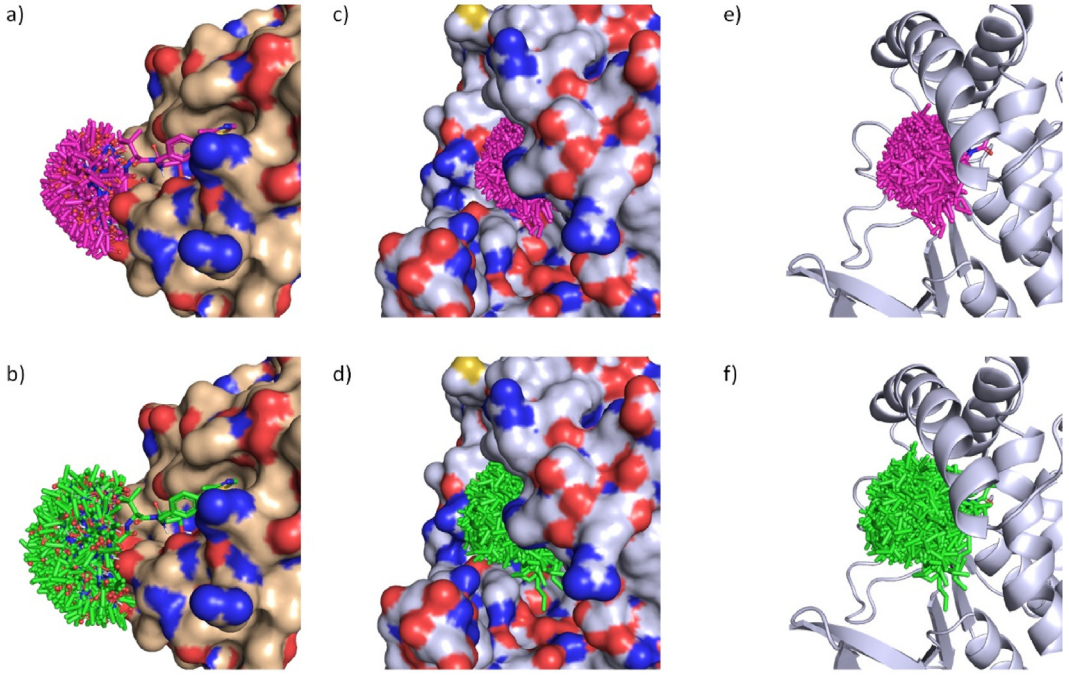

Fig. 2. Model of the linker exposure in VHL E3 ligase (extracted from PDB ID: 5T35, wheat color) and in human mPGES-2 (from homology model, grey color. See experimental section for details). **(a)** spatial distribution of linker in the VHL-linker moiety from **2**. **(b)** spatial distribution of linker in the VHL-linker moiety from **3**. **(c)** and **(e)** spatial distribution of linker in the INM-linker moiety from **2** in surface and cartoon modes, respectively. **(d)** and **(f)** spatial distribution of linker in the INM-linker moiety from **3** in surface and cartoon modes, respectively.

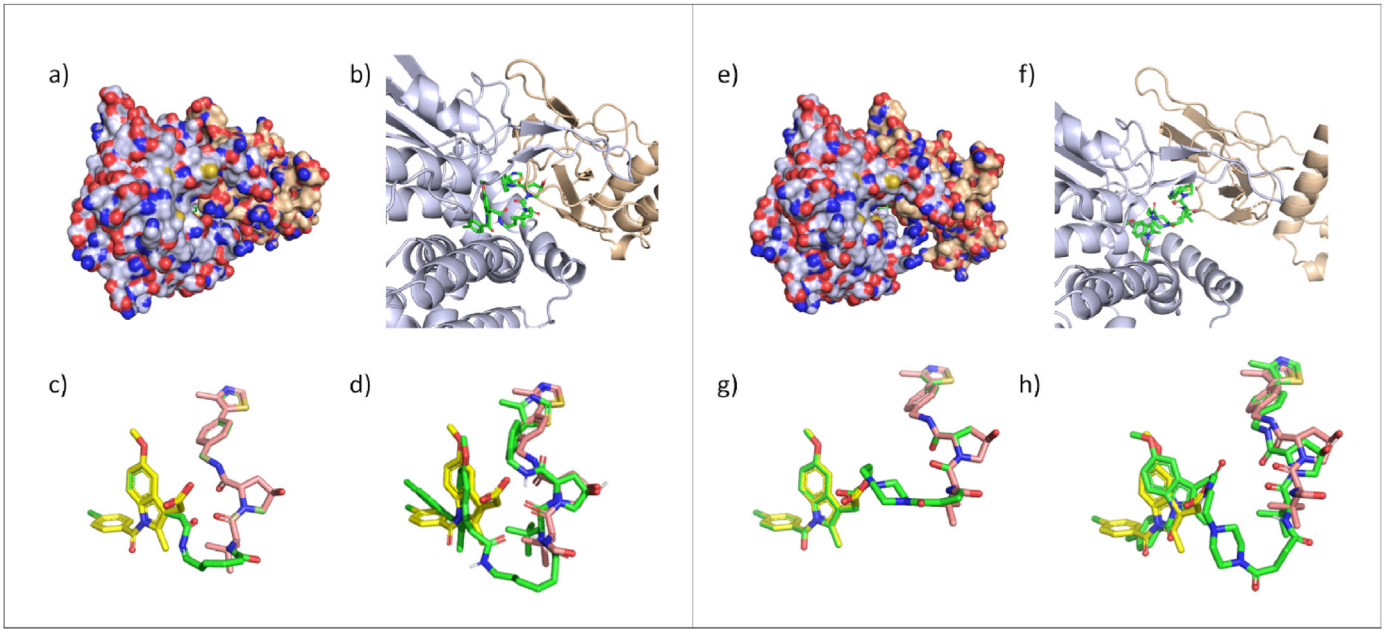

Fig. 3. Model of the PGES-2/Compound **3**/E3 and PGES-2/Compound **5**/E3 ternary complexes. **(a)** and **(e)** visualization of the complex in surface mode (VHL E3 ligase and human mPGES-2 in wheat and grey, respectively); **(b)** detail of the complex showing the region of the PGES-2/Compound **3**/E3 interaction; **(c)** pose of **3** with ligand moieties overlapping the corresponding ligands in the E3 ligase x-ray structure (salmon color) and in the human mPGES-2 homology model (yellow color) (pre-optimization); **(d)** pose of **3** after optimization of the overall ternary complex; **(f)** detail of the complex showing the region of the PGES-2/Compound **5**/E3 interaction; **(g)** pose of **5** with ligand moieties overlapping the corresponding ligands in the E3 ligase x-ray structure (salmon color) and in the human mPGES-2 homology model (yellow color) (pre-optimization); **(h)** pose of **5** after optimization of the overall ternary complex.

application in the context of coronavirus inhibition, in which a human host protein rather than a viral one was exploited as a target. Indeed, host-directed antivirals should have an advantage in overcoming resistance issues related to the emergence of mutations in the viral genome that might make the virus less susceptible to some inhibitors without affecting viral fitness [48,49]. This is an important issue, in particular with RNA viruses such as CoVs. Being inspired by a recent work in which the weak

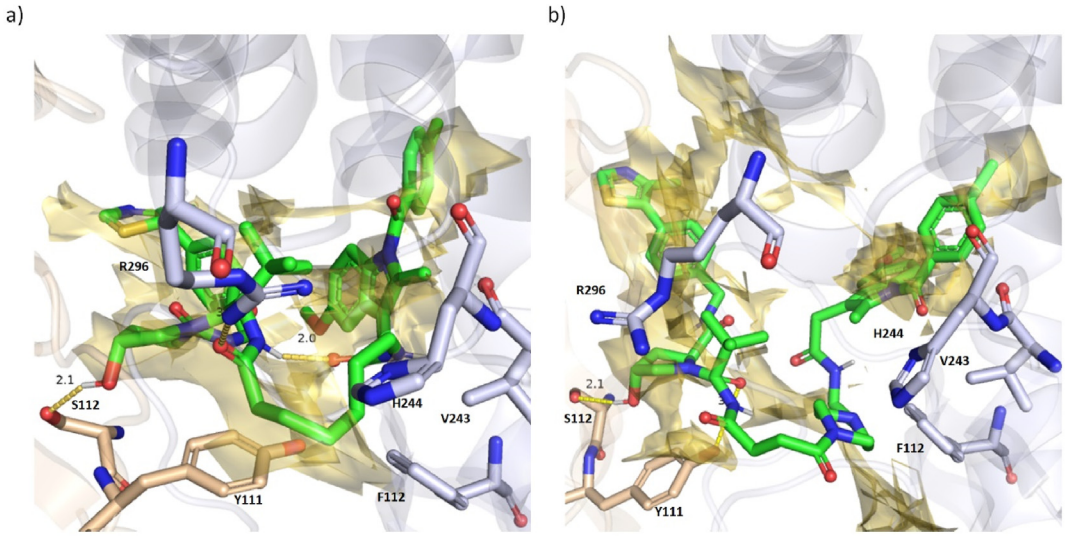

Fig. 4. Predicted poses of compounds **3** (a) and **5** (b) in the ternary complexes. Hydrophobic regions calculated using the CRY probe in the GRID software [46,47] are highlighted as yellow surfaces. VHL E3 ligase (extracted from PDB ID: 5T35) and in human mPGES-2 homology model are shown in wheat and grey color respectively.

anti-SARS-CoV-2 activity of INM was hypothesized to be linked to its ability to bind and inhibit PGES-2, a host protein which interacts with SARS-CoV-2 NSP7 protein, we synthesized four first-in-class INM-based PROTACs bearing the VHL E3 ligase ligand and varying the linker moiety. As known, for the design of PROTACs high-affinity POI ligands or potent inhibitors are not strictly required since only the binding to the protein target is needed in order to permit the ternary complex formation that is responsible for subsequent proteasomal-dependent POI degradation. Biological evaluation of the four INM-based PROTACs showed that compounds **3** (endowed with a 6-methylene-unit linker) and **5** (endowed with a piperazine-based linker) were about 4.5-fold more potent than INM. In addition, they exhibited a broad-spectrum inhibitory activity toward two different SARS-CoV-2 strains, along with different human CoVs: the β-coronavirus HCoV-OC43 (EC_{50} = 4.7 μM and 2.5 μM, respectively) and the α-coronavirus HCoV-229E (EC_{50} = 36.5 μM and EC_{50} = 3.4 μM, respectively), proving that both compounds **3** and **5** exhibit broad-spectrum antiviral activity against pandemic and epidemic CoVs belonging to different genera of *Coronaviridae* family. Moreover, INM-derived PROTACs **3** and **5** resulted in general more active against HCoVs compared to SARS-CoV-2, and further studies will be aimed at investigating this aspect, which may be due to possible differences in E3 ligase VHL expression as well as in the expression and/or activity of the target PGES-2 in the two different cell lines used in the experiments. Molecular modelling studies were performed to further interpret the experimental outcomes and led to hypothesize that a linker of 6-methylene units or other linkers of equivalent length allow the formation of PGES-2/INM-derived PROTAC/E3 ternary complex, while shorter linkers make the interaction unfavourable. In addition, the predicted pose for compounds **3** and **5** in the corresponding ternary complexes was studied, representing valuable information for future rational design and hit-to-lead optimization. In particular, the exploration of further aliphatic and piperazine-containing linkers and different E3 ligase ligands along with an in-depth investigation of the role of PGES-2 in SARS-CoV-2 replicative cycle will be the object of the successive study.

In summary, this study represents the proof-of-concept of PROTACs-based antiviral drug discovery in the field of coronaviruses and paves the way toward the use of indomethacin derivatives for the development of new pan-CoV antivirals that could contribute to fill the gap in the lack of effective anti-CoV drugs. To the best of our knowledge, this is the first example of the application of small molecule degraders in the development of CoV antiviral drugs.

4. Experimental section

4.1. General synthetic chemistry methods

Unless otherwise noted, starting materials, reagents, and solvents were purchased from commercial suppliers and were used as received without further purification. Indomethacin (**1**) was purchased by Fluorochem.

Reactions were routinely monitored by thin-layer chromatography (TLC) performed on silica gel 60 F254 (layer 0.2 mm) precoated aluminium foil (with fluorescent indicator UV254) (Sigma-Aldrich). Developed plates were air-dried and visualized by UV detector (λ: 254/365 nm) and/or by staining and warming with potassium permanganate or ninhydrin. Flash column chromatography was performed on Merck silica gel 60 (mesh 230–400). Automated flash chromatographic purifications were performed using Biotage® Selekt (Cartridge: Sfär Silica HC Duo 5g or 10g). ^{1}H NMR and ^{13}C NMR spectra were recorded at room temperature at 400 and 101 MHz, respectively, on a Bruker Avance 400 spectrometer in the indicated solvent by using TMS or residual solvent peak as internal standard. Chemical shifts are reported in ppm (δ) and the coupling constants (J) are given in Hertz (Hz). Peak multiplicities are abbreviated as follows: s (singlet), bs (broad singlet), d (doublet), dd (double doublet), t (triplet), dt (double triplet), q (quartet), p (pentet), and m (multiplet). High-Resolution Mass Spectroscopy (HRMS) analyses were carried out on Agilent Technologies 6540 UHD Accurate Mass Q-TOF LC-MS system. The purity of all synthesized compounds was confirmed to be >95% by UPLC-MS. The analyses were carried out according to the method listed below. The mobile phase was a mixture of water (solvent A) and acetonitrile (solvent B), both containing formic acid at 0.1%. Method: Acquity UPLC BEH C18 1.7 μm (C18, 150 × 2.1 mm) column at 40 °C using a flow rate of 0.65 mL/min in a 10 min gradient elution. Gradient elution was as follows: 99.5:0.5 (A/B) to 5:95 (A/B) over 8 min, 5:95 (A/B) for 2 min, and then reversion back to 99.5:0.5 (A/B) over 0.1 min. The UV detection is an averaged signal from a

wavelength of 190 nm–640 nm and mass spectra are recorded on a mass spectrometer using positive mode electro spray ionization. The chemical names were generated using ChemBioDraw 12.0 from CambridgeSoft.

4.1.1. General Procedure A (HATU-mediated reaction)

Under nitrogen atmosphere, to a stirred solution of indomethacin (1.0 equiv), suitable amino containing VHL-linker intermediate (1.0 equiv), and DIPEA (3.0 equiv) in dry DMF, HATU (1.25 eq) was added and the reaction mixture was stirred at room temperature (5–18h). The mixture was poured in ice-water yielding a precipitate collected by filtration. The crude was purified as described below.

4.1.2. (2S,4R)-1-((S)-2-(5-(2-(1-(4-chlorobenzoyl)-5-methoxy-2-methyl-1H-indol-3-yl)acetamido)pentanamido)-3,3-dimethylbutanoyl)-4-hydroxy-N-((S)-1-(4-(4-methylthiazol-5-yl)phenyl)ethyl)pyrrolidine-2-carboxamide (2)

General Procedure A (16h) was followed by using **1** (0.030 g, 0.084 mmol) and VHL-linker intermediate **15** [44] (0.049 g, 0.084 mmol) to afford the titled compound as light-yellow solid (20.5 mg, 28% yield) after purification by automated flash chromatography on SiO_2 cartridge (DCM/MeOH from to 99:1 to 95:5, v/v). ^{1}H NMR (400 MHz, $CDCl_3$) δ 8.72 (s, 1H), 7.66 (d, J = 8.3 Hz, 2H), 7.47 (d, J = 8.3 Hz, 2H), 7.44–7.28 (m, 5H), 6.97 (d, J = 2.3 Hz, 1H), 6.91 (d, J = 9.0 Hz, 1H), 6.69 (dd, J = 8.9, 2.3 Hz, 1H), 6.34 (d, J = 8.8 Hz, 1H), 5.92 (t, J = 5.9 Hz, 1H), 5.13–5.02 (m, 1H), 4.73 (t, J = 8.0 Hz, 1H), 4.51 (d, J = 8.9 Hz, 1H), 4.46 (s, 1H), 4.02 (d, J = 11.7 Hz, 1H), 3.80 (s, 3H), 3.72–3.57 (m, 2H), 3.53 (dd, J = 11.3, 3.3 Hz, 1H), 3.32–3.19 (m, 1H), 3.14–3.00 (m, 1H), 2.62–2.46 (m, 4H), 2.36 (s, 3H), 2.20 (t, J = 6.7 Hz, 2H), 2.12–2.00 (m, 1H), 1.61–1.50 (m, 2H), 1.49–1.35 (m, 5H), 1.01 (s, 9H); ^{13}C NMR (101 MHz, $CDCl_3$) δ 173.43, 172.18, 170.40, 169.69, 168.53, 156.27, 150.45, 147.77, 143.47, 139.59, 136.54, 133.61, 131.29, 131.18 (2C), 130.99, 130.48, 130.38, 129.54 (2C), 129.24 (2C), 126.51 (2C), 115.11, 112.86, 112.11, 101.26, 70.00, 58.35, 57.52, 56.89, 55.84, 48.86, 38.52, 35.39, 35.18, 35.11, 32.09, 28.47, 26.49 (3C), 22.25, 21.87, 15.79, 13.40. HRMS (ESI) m/z [M+H]+ calcd for $C_{47}H_{55}ClN_6O_7S$ 883.36142, found 883.36275. UPLC retention time: 5.643 min.

4.1.3. (2S,4R)-1-((S)-2-(7-(2-(1-(4-chlorobenzoyl)-5-methoxy-2-methyl-1H-indol-3-yl)acetamido)heptanamido)-3,3-dimethylbutanoyl)-4-hydroxy-N-((S)-1-(4-(4-methylthiazol-5-yl)phenyl)ethyl)pyrrolidine-2-carboxamide (3)

General Procedure A (16h) was followed by using **1** (0.050 g, 0.139 mmol) and VHL-linker intermediate **16** [44] (0.085 g, 0.139 mmol) to afford the titled compound as light-yellow solid (38 mg, 31% yield) after purification by automated flash chromatography on SiO_2 (DCM/MeOH from 98:2 to 96:4, v/v). ^{1}H NMR (400 MHz, $CDCl_3$) δ 8.67 (s, 1H), 7.66 (d, J = 8.3 Hz, 2H), 7.52 (d, J = 8.0 Hz, 1H), 7.48 (d, J = 8.2 Hz, 2H), 7.44–7.34 (m, 4H), 6.93 (d, J = 2.4 Hz, 1H), 6.87 (d, J = 9.1 Hz, 1H), 6.69 (dd, J = 9.2, 2.0 Hz, 1H), 6.27 (d, J = 8.3 Hz, 1H), 5.77–5.68 (m, 1H), 5.14–5.03 (m, 1H), 4.74 (t, J = 7.9 Hz, 1H), 4.57 (d, J = 8.6 Hz, 1H), 4.47 (s, 1H), 4.13 (d, J = 11.7 Hz, 1H), 3.82 (s, 3H), 3.62 (s, 2H), 3.57 (dd, J = 11.4, 3.2 Hz, 1H), 3.16 (dd, J = 13.5, 7.1 Hz, 2H), 2.59–2.43 (m, 4H), 2.37 (s, 3H), 2.26–2.02 (m, 3H), 1.65–1.44 (m, 5H), 1.44–1.29 (m, 2H), 1.30–1.14 (m, 4H), 1.04 (s, 9H); ^{13}C NMR (101 MHz, $CDCl_3$) δ 173.76, 172.16, 170.04, 169.77, 168.41, 156.20, 150.33, 148.46, 143.26, 139.63, 136.41, 133.56, 131.63, 131.22 (2C), 130.96, 130.84, 130.37, 129.57 (2C), 129.25 (2C), 126.45 (2C), 115.10, 112.89, 112.06, 101.15, 69.99, 58.32, 57.59, 56.77, 55.77, 48.86, 39.33, 35.96, 35.56, 34.89, 32.22, 29.05, 28.16, 26.53 (3C), 26.06, 25.14, 22.29, 16.08, 13.30. HRMS (ESI) m/z [M+H]+ calcd for $C_{49}H_{59}ClN_6O_7S$ 911.39272, found 911.39345. UPLC retention time: 5.825 min.

4.1.4. (2S,4R)-1-((S)-2-(tert-butyl)-14-(1-(4-chlorobenzoyl)-5-methoxy-2-methyl-1H-indol-3-yl)-4,13-dioxo-6,9-dioxa-3,12-diazatetradecanoyl)-4-hydroxy-N-((S)-1-(4-(4-methylthiazol-5-yl)phenyl)ethyl)pyrrolidine-2-carboxamide (4)

General Procedure A (5h) was followed by using **1** (0.050 g, 0.139 mmol) and VHL-linker intermediate **17** [44] (0.087 g, 0.139 mmol) to afford the titled compound as light-yellow solid (22 mg, 17% yield) after purification by automated flash chromatography on SiO_2 cartridge (DCM/MeOH 98:2 to 96:4, v/v). ^{1}H NMR (400 MHz, $CDCl_3$) δ 8.81 (s, 1H), 7.63 (d, J = 8.0 Hz, 2H), 7.47 (d, J = 7.9 Hz, 3H), 7.40 (d, J = 7.9 Hz, 2H), 7.31 (d, J = 7.8 Hz, 2H), 7.04 (d, J = 9.0 Hz, 1H), 6.96 (s, 1H), 6.81 (s, 1H), 6.72 (d, J = 8.8 Hz, 1H), 6.59 (d, J = 7.7 Hz, 1H), 5.08–4.96 (m, 1H), 4.67 (d, J = 9.2 Hz, 1H), 4.47 (s, 1H), 4.31 (t, J = 7.9 Hz, 1H), 3.99–3.43 (m, 16H), 3.40–3.32 (m, 1H), 2.56 (s, 3H), 2.40–2.27 (m, 4H), 2.09–2.00 (m, 1H), 1.40 (d, J = 6.8 Hz, 3H), 1.01 (s, 9H). HRMS (ESI) m/z [M+H]+ calcd for $C_{48}H_{57}ClN_6O_9S$ 929.36690, found 929.36968. UPLC retention time: 5.971 min.

4.1.5. (2S,4R)-1-((S)-2-(4-(4-(2-(2-(1-(4-chlorobenzoyl)-5-methoxy-2-methyl-1H-indol-3-yl)acetamido)ethyl)piperazin-1-yl)-4-oxobutanamido)-3,3-dimethylbutanoyl)-4-hydroxy-N-((S)-1-(4-(4-methylthiazol-5-yl)phenyl)ethyl)pyrrolidine-2-carboxamide (5)

General Procedure A (16h) was followed by using **1** (0.050 g, 0.139 mmol) and VHL-linker intermediate **18** (0.097 g, 0.139 mmol) to afford the titled compound as light-yellow solid (34 mg, 24% yield) after purification by automated flash chromatography on SiO_2 cartridge (DCM/MeOH 98:2 to 96:4, v/v). ^{1}H NMR (400 MHz, $CDCl_3$) δ 8.66 (s, 1H), 7.64 (d, J = 8.4 Hz, 3H), 7.47 (d, J = 8.5 Hz, 2H), 7.43–7.31 (m, 4H), 6.88 (dd, J = 11.5, 5.9 Hz, 3H), 6.69 (dd, J = 9.1, 2.3 Hz, 1H), 6.21 (s, 1H), 5.16–5.01 (m, 1H), 4.73 (t, J = 8.3 Hz, 1H), 4.49–4.34 (m, 2H), 4.10–3.99 (m, 1H), 3.82 (s, 3H), 3.63 (s, 2H), 3.56 (dd, J = 11.3, 2.7 Hz, 1H), 3.36–3.01 (m, 6H), 2.70–2.06 (m, 18H), 1.48 (d, J = 6.9 Hz, 3H), 1.05 (s, 9H); ^{13}C NMR (101 MHz, $CDCl_3$) δ 173.24, 171.96, 170.35, 169.99 (2C), 168.47, 156.24, 150.26, 148.45, 143.47, 139.68, 136.23, 133.48, 131.61, 131.21 (2C), 130.95, 130.76, 130.37, 129.51 (2C), 129.27 (2C), 126.41 (2C), 115.02, 113.04, 111.98, 101.22, 77.34, 77.02, 76.70, 70.11, 58.46, 58.40, 56.62, 56.05, 55.80, 52.34, 52.06, 48.82, 45.01, 41.66, 36.18, 35.87, 34.78, 32.12, 30.77, 28.30, 26.51 (3C), 22.22, 16.11, 13.28. HRMS (ESI) m/z [M+H]+ calcd for $C_{52}H_{63}ClN_8O_8S$ 995.42563, found 995.42844. UPLC retention time: 4.834 min.

4.1.6. 4-(4-(2-((Tert-butoxycarbonyl)amino)ethyl)piperazin-1-yl)-4-oxobutanoic acid (10)

Under nitrogen atmosphere, to the solution of succinic anhydride (0.150 g, 0.654 mmol) in dry DCM (3.0 mL) was added *tert*-butyl (2-(piperazin-1-yl)ethyl)carbamate (0.065 g, 0.654 mmol) and the resulting mixture was stirred at room temperature for 4 h. The solvent was evaporated to dryness affording the titled compound as colourless oil (0.215 g, 100% yield). ^{1}H NMR (400 MHz, MeOD) δ 3.62–3.55 (m, 4H), 3.21 (t, J = 6.6 Hz, 2H), 2.68–2.63 (m, 2H), 2.61–2.54 (m, 4H), 2.54–2.47 (m, 4H), 1.44 (s, 9H).

4.1.7. Tert-butyl (2-(4-(4-(((S)-1-((2S,4R)-4-hydroxy-2-(((S)-1-(4-(4-methylthiazol-5-yl)phenyl)ethyl)carbamoyl)pyrrolidin-1-yl)-3,3-dimethyl-1-oxobutan-2-yl)amino)-4-oxobutanoyl)piperazin-1-yl)ethyl)carbamate (14)

General Procedure A (18h) was followed by using **10** (0.195 g, 0.592 mmol) and **6** (0.294 mg, 0.592 mmol) to afford the titled compound as white solid (0.266 g, 50% yield) after purification by flash column chromatography on SiO_2 (DCM/MeOH, 9:1 to 8:2). ^{1}H NMR (400 MHz, DMSO-d_6) δ 8.98 (s, 1H), 8.37 (d, J = 7.8 Hz, 1H), 7.86 (d, J = 9.2 Hz, 1H), 7.47–7.34 (m, 4H), 6.78 (s, 1H), 5.09 (d, J = 3.0 Hz, 1H), 4.92 (dd, J = 14.0, 6.8 Hz, 1H), 4.49 (d, J = 9.3 Hz, 1H), 4.42 (t,

J = 8.1 Hz, 1H), 4.28 (s, 1H), 3.65–3.40 (m, 5H), 3.32 (s, 3H), 3.20–3.06 (m, 3H), 2.45 (s, 4H), 2.42–2.26 (m, 2H), 2.05–1.96 (m, 1H), 1.85–1.74 (m, 1H), 1.48–1.28 (m, 12H), 1.28–1.19 (m, 1H), 0.93 (s, 9H).

4.1.8. (2S,4R)-1-((S)-2-(4-(4-(2-aminoethyl)piperazin-1-yl)-4-oxobutanamido)-3,3-dimethylbutanoyl)-4-hydroxy-N-((S)-1-(4-(4-methylthiazol-5-yl)phenyl)ethyl)pyrrolidine-2-carboxamide hydrochloride (18)

A solution of HCl 4 N in dioxane (2.3 mL) was added to **14** (0.225 g, 0.298 mmol) and the resulting mixture was stirred at room temperature overnight. The solvent was then evaporated to dryness and the solid tritured with DEE and collected by filtration, to afford the titled compound (0.200 g, 97% yield) as white solid. ^{1}H NMR (400 MHz, DMSO-d_6) δ 8.99 (s, 1H), 8.39 (d, J = 7.8 Hz, 1H), 8.25 (bs, 3H), 7.89 (d, J = 8.9 Hz, 1H), 7.43 (d, J = 8.2 Hz, 2H), 7.38 (d, J = 8.3 Hz, 2H), 4.95–4.88 (m, 1H), 4.50 (d, J = 9.4 Hz, 1H), 4.42 (t, J = 8.3 Hz, 1H), 4.28 (s, 1H), 3.64–3.53 (m, J = 16.0 Hz, 11H), 2.65–2.54 (m, J = 10.2 Hz, 4H), 2.45 (s, 3H), 2.07–1.96 (m, J = 9.7 Hz, 1H), 1.83–1.73 (m, 1H), 1.37 (d, J = 6.9 Hz, 3H), 1.30–1.21 (m, 1H), 0.94 (s, 9H).

4.2. Biological activity

4.2.1. Plaque reduction assays

Plaque reduction assays (PRAs) with different CoVs were performed as follows. For SARS-CoV-2 infection, Vero E6 cells (ATCC® CRL-1586™) were seeded at a density of 1×10^5 cells per well in 24-well plates. The next day, the cells were infected with 80 Plaque Forming Unit (PFU) per well of the different SARS-CoV-2 strains (SARS-CoV-2/NL/2020 and a clinical isolate SARS-CoV-2/Padova/2021). After incubation, the inoculum was removed, and media containing various concentrations of each compound, 3% FBS, and 0.6% methylcellulose were added. After 3 days of incubation, cell monolayers were fixed and stained, and viral plaques were counted. For infection with HCoV-OC43 (ATCC® VR-1558™) and HCoV-229E (ATCC® VR-740™) strains, MRC-5 cells (ATCC® CCL-171™) were seeded at a density of 6×10^4 cells per well in 24-well plates. The next day, the cells were infected with 80 Plaque Forming Unit (PFU) per well of the different HCoVs. After incubation, the inoculum was removed, and media containing various concentrations of each compound, 3% FBS, and 0.6% methylcellulose were added. After 3 days of incubation, cell monolayers were fixed and stained, and viral plaques were counted. All work with infectious SARS-CoV-2 viruses was performed in a biosafety level 3 (BSL3) laboratory according to the safety practices as approved by the Department of Molecular Medicine (University of Padova, Italy) Committee on Microbiological Safety.

4.2.2. Cell viability assays

The effect on cell viability of test compounds was determined in Vero E6 and MRC-5 cells at 72 h by the 3-(4,5-dimethylthiazol-2-yl)-2,5-diphenyl tetrazolium bromide (MTT; Sigma-Aldrich) method as described previously [50].

4.3. Modelling studies

The crystallographic structure of human PGES-2 is not available in the Protein Data Bank [51]. Therefore, in order to model its interaction with indomethacin, we used a homology model obtained from the *Macaca fascicularis* PGES-2 crystallographic structure, since the two proteins show a sequence homology of 98.94% (a focus on the overlap of the INM binding site between the two proteins is showed in Figure S2). A homology model of human PGEs, obtained from the *Macaca fascicularis* crystallographic structure in bound form (PDB ID: 2PBJ), was already available on the SWISS-MODEL repository [52], a database of annotated 3D protein structure models generated by the SWISS-MODEL homology-modeling pipeline. This model contains, as 2PBJ template, the heme and the glutathione groups. We aligned the homology model obtained from SWISS-MODEL repository with another crystallographic structure of *Macaca fascicularis* PGES bound with INM (PDB ID: 1Z9H) (Figure S2). The indomethacin binding site coincides with the heme and glutathione binding site. Heme and glutathione were then removed from the structure since it is not known if they are required for prostaglandin synthase activity, and it has been hypothesized that both GSH-heme complex-free and -bound enzymes are present in the same tissues [53,54]. Finally, we extracted the indomethacin pose from 1Z9H structures and used it within the human homology model structure.

The x-ray structure of VHL E3 ligase in complex with its ligand was extracted from the PDB ID 5T35 (The PROTAC MZ1 in complex with the second bromodomain of Brd4 and pVHL:ElonginC:ElonginB) [55].

To evaluate the effect of the length of the aliphatic linker, the linker under investigation was first attached to the VHL ligand, and then all the potential conformers of the linker-VHL moiety were generated by fixing the pose of the VHL ligand in its x-ray pose. The procedure was then repeated this time attaching the linker to INM moiety and then generating all the potential conformers of the linker-INM moiety with the INM molecule fixed in its pose resulted from the used homology model. Finally, from the two sets of conformations generated, the pairs that were compatible were selected, that is, those that allowed optimal contacts, without repulsive steric interactions between the INM-linker-VHL complex with the respective protein structures. To hypothesize the formation of the PGES-2/PROTAC/E3 ternary complex, GRID Molecular Interaction Fields (MIFs) [46,47,56] were calculated at the PGES-2 and VHL-E3 ligase protein surfaces in the proximity of the binding site, and the best complementarity of the hydrophobic and polar MIFs was used as the driving force of the ternary complex formation. Once the best orientation was found, the PROTAC was docked by overlapping the ligands onto the x-ray poses and adjusting the linker to get rid of clashes and to optimize interactions. To generate the hydrophobic MIF the CRY probe was used [57], while polar interactions were evaluated using the N1 and the O probes, all within the GRID 2021 package [56].

Declaration of competing interest

The authors declare that they have no known competing financial interests or personal relationships that could have appeared to influence the work reported in this paper.

Acknowledgements

This work was supported by Fondazione Cassa di Risparmio di Padova e Rovigo, Italy – Bando Ricerca Covid-2019 Nr. 55777 2020.0162 – ARREST-COV: AntiviRal PROTAC-Enhanced Small-molecule Therapeutics against CoronaViruses" (to A.L.); by Fondazione Cassa di Risparmio di Foligno, Italy – "PANCRAS: PROTACs and Corona Virus" (to G.C.); by The Universita degli Studi di Perugia, Italy and MIUR-project AMIS, through the program "Dipartimenti di Eccellenza-2018–2022" (to G.C. and L.G.); by Associazione Italiana per la Ricerca sul Cancro, Italy (AIRC, grant n. IG18855 to A.L.); by Ministero dell'Istruzione, dell'Università e della Ricerca, Italy (PRIN 2017 n. 2017KM79NN to A.L.); by British Society for Antimicrobial Chemotherapy, UK (grant BSAC-2018-0064 to A.L.); by Fondazione Umberto Veronesi, Italy (to M.C.). This publication was also supported by the European Virus Archive Global (EVA-GLOBAL)

project, which has received funding from the European Union's Horizon 2020 research and innovation programme under grant agreement No 871029 and provided free access to the SARS-CoV-2/NL/2020 virus. The funders had no role in study design, data collection and interpretation, or the decision to submit the work for publication. The authors thank Dr. Simon Cross for English revision.

Appendix A. Supplementary data

Supplementary data associated with this article can be found in the online version, at https://doi.org/10.1016/j.ejmech.2021.113814. These data include MOL files and InChiKeys of the most important compounds described in this article.

References

[1] P. Zhou, X.L. Yang, X.G. Wang, B. Hu, L. Zhang, W. Zhang, H.R. Si, Y. Zhu, B. Li, C.L. Huang, H.D. Chen, J. Chen, Y. Luo, H. Guo, R.D. Jiang, M.Q. Liu, Y. Chen, X.R. Shen, X. Wang, X.S. Zheng, K. Zhao, Q.J. Chen, F. Deng, L.L. Liu, B. Yan, F.X. Zhan, Y.Y. Wang, G.F. Xiao, Z.L. Shi, A pneumonia outbreak associated with a new coronavirus of probable bat origin, Nature 579 (2020) 270–273.

[2] N. Zhu, D. Zhang, W. Wang, X. Li, B. Yang, J. Song, X. Zhao, B. Huang, W. Shi, R. Lu, P. Niu, F. Zhan, X. Ma, D. Wang, W. Xu, G. Wu, G.F. Gao, W. Tan, I. China Novel Coronavirus, T. Research, A novel coronavirus from patients with pneumonia in China, The New England journal of medicine 382 (2019) 727–733, 2020.

[3] WHO coronavirus (COVID-19) dashboard. https://covid19.who.int/.

[4] R. Lu, X. Zhao, J. Li, P. Niu, B. Yang, H. Wu, W. Wang, H. Song, B. Huang, N. Zhu, Y. Bi, X. Ma, F. Zhan, L. Wang, T. Hu, H. Zhou, Z. Hu, W. Zhou, L. Zhao, J. Chen, Y. Meng, J. Wang, Y. Lin, J. Yuan, Z. Xie, J. Ma, W.J. Liu, D. Wang, W. Xu, E.C. Holmes, G.F. Gao, G. Wu, W. Chen, W. Shi, W. Tan, Genomic characterisation and epidemiology of 2019 novel coronavirus: implications for virus origins and receptor binding, Lancet 395 (2020) 565–574.

[5] Y. Chen, Q. Liu, D. Guo, Emerging coronaviruses: genome structure, replication, and pathogenesis, Journal of medical virology 92 (2020) 418–423.

[6] F. Wu, S. Zhao, B. Yu, Y.M. Chen, W. Wang, Z.G. Song, Y. Hu, Z.W. Tao, J.H. Tian, Y.Y. Pei, M.L. Yuan, Y.L. Zhang, F.H. Dai, Y. Liu, Q.M. Wang, J.J. Zheng, L. Xu, E.C. Holmes, Y.Z. Zhang, A new coronavirus associated with human respiratory disease in China, Nature 579 (2020) 265–269.

[7] S. Su, G. Wong, W. Shi, J. Liu, A.C.K. Lai, J. Zhou, W. Liu, Y. Bi, G.F. Gao, Epidemiology, genetic recombination, and pathogenesis of coronaviruses, Trends in microbiology 24 (2016) 490–502.

[8] Remdesivir emergency use authorization; gilead sciences, inc. https://www.gilead.com/media/files/pdfs/remdesivir.

[9] C.C. Lai, C.H. Chen, C.Y. Wang, K.H. Chen, Y.H. Wang, P.R. Hsueh, Clinical efficacy and safety of remdesivir in patients with COVID-19: a systematic review and network meta-analysis of randomized controlled trials, The Journal of antimicrobial chemotherapy (2021).

[10] Solidarity" clinical trial for COVID-19 treatments. https://www.who.int/emergencies/diseases/novel-coronavirus-2019/global-research-on-novel-coronavirus-2019-ncov/solidarity-clinical-trial-for-covid-19-treatments.

[11] E. Calvo Fernandez, L.Y. Zhu, Racing to immunity: journey to a COVID-19 vaccine and lessons for the future, British journal of clinical pharmacology (2020).

[12] S. Kotta, H.M. Aldawsari, S.M. Badr-Eldin, N.A. Alhakamy, Md S, A.B. Nair, P.K. Deb, Combating the pandemic COVID-19: clinical trials, therapies and perspectives, Frontiers in molecular biosciences 7 (2020) 606393.

[13] J. Xu, Y. Xue, R. Zhou, P.Y. Shi, H. Li, J. Zhou, Drug Repurposing Approach to Combating Coronavirus: Potential Drugs and Drug Targets, Medicinal research reviews, 2020.

[14] R. Cannalire, C. Cerchia, A.R. Beccari, F.S. Di Leva, V. Summa, Targeting SARS-CoV-2 proteases and polymerase for COVID-19 treatment: state of the art and future opportunities, J Med Chem (2020).

[15] P.N. Batalha, L.S.M. Forezi, C.G.S. Lima, F.P. Pauli, F.C.S. Boechat, M. de Souza, A.C. Cunha, V.F. Ferreira, F.C. da Silva, Drug repurposing for the treatment of COVID-19: pharmacological aspects and synthetic approaches, Bioorganic chemistry 106 (2021) 104488.

[16] J. Trivedi, M. Mohan, S.N. Byrareddy, Drug repurposing approaches to combating viral infections, Journal of clinical medicine 9 (2020).

[17] B. Mercorelli, G. Palu, A. Loregian, Drug repurposing for viral infectious diseases: how far are we? Trends in microbiology 26 (2018) 865–876.

[18] M.A. Marinella, Indomethacin and resveratrol as potential treatment adjuncts for SARS-CoV-2/COVID-19, International journal of clinical practice 74 (2020), e13535.

[19] T. Xu, X. Gao, Z. Wu, D.W. Selinger, Z. Zhou, Indomethacin Has a Potent Antiviral Activity against SARS CoV-2 in Vitro and Canine Coronavirus in Vivo, bioRxiv, 2020.

[20] X. Zeng, X. Song, T. Ma, X. Pan, Y. Zhou, Y. Hou, Z. Zhang, K. Li, G. Karypis, F. Cheng, Repurpose open data to discover therapeutics for COVID-19 using deep learning, Journal of proteome research 19 (2020) 4624–4636.

[21] D.E. Gordon, G.M. Jang, M. Bouhaddou, J. Xu, K. Obernier, K.M. White, M.J. O'Meara, V.V. Rezelj, J.Z. Guo, D.L. Swaney, T.A. Tummino, R. Huttenhain, R.M. Kaake, A.L. Richards, B. Tutuncuoglu, H. Foussard, J. Batra, K. Haas, M. Modak, M. Kim, P. Haas, B.J. Polacco, H. Braberg, J.M. Fabius, M. Eckhardt, M. Soucheray, M.J. Bennett, M. Cakir, M.J. McGregor, Q. Li, B. Meyer, F. Roesch, T. Vallet, A. Mac Kain, L. Miorin, E. Moreno, Z.Z.C. Naing, Y. Zhou, S. Peng, Y. Shi, Z. Zhang, W. Shen, I.T. Kirby, J.E. Melnyk, J.S. Chorba, K. Lou, S.A. Dai, I. Barrio-Hernandez, D. Memon, C. Hernandez-Armenta, J. Lyu, C.J.P. Mathy, T. Perica, K.B. Pilla, S.J. Ganesan, D.J. Saltzberg, R. Rakesh, X. Liu, S.B. Rosenthal, L. Calviello, S. Venkataramanan, J. Liboy-Lugo, Y. Lin, X.P. Huang, Y. Liu, S.A. Wankowicz, M. Bohn, M. Safari, F.S. Ugur, C. Koh, N.S. Savar, Q.D. Tran, D. Shengjuler, S.J. Fletcher, M.C. O'Neal, Y. Cai, J.C.J. Chang, D.J. Broadhurst, S. Klippsten, P.P. Sharp, N.A. Wenzell, D. Kuzuoglu-Ozturk, H.Y. Wang, R. Trenker, J.M. Young, D.A. Cavero, J. Hiatt, T.L. Roth, U. Rathore, A. Subramanian, J. Noack, M. Hubert, R.M. Stroud, A.D. Frankel, O.S. Rosenberg, K.A. Verba, D.A. Agard, M. Ott, M. Emerman, N. Jura, M. von Zastrow, E. Verdin, A. Ashworth, O. Schwartz, C. d'Enfert, S. Mukherjee, M. Jacobson, H.S. Malik, D.G. Fujimori, T. Ideker, C.S. Craik, S.N. Floor, J.S. Fraser, J.D. Gross, A. Sali, B.L. Roth, D. Ruggero, J. Taunton, T. Kortemme, P. Beltrao, M. Vignuzzi, A. Garcia-Sastre, K.M. Shokat, B.K. Shoichet, N.J. Krogan, A SARS-CoV-2 protein interaction map reveals targets for drug repurposing, Nature 583 (2020) 459–468.

[22] P.P. Rao, S.N. Kabir, T. Mohamed, Nonsteroidal anti-inflammatory drugs (NSAIDs): progress in small molecule drug development, Pharmaceuticals 3 (2010) 1530–1549.

[23] T. Yamada, J. Komoto, K. Watanabe, Y. Ohmiya, F. Takusagawa, Crystal structure and possible catalytic mechanism of microsomal prostaglandin E synthase type 2 (mPGES-2), Journal of molecular biology 348 (2005) 1163–1176.

[24] L. Kaplan, J. Weiss, P. Elsbach, Low concentrations of indomethacin inhibit phospholipase A2 of rabbit polymorphonuclear leukocytes, Proc Natl Acad Sci U S A 75 (1978) 2955–2958.

[25] R.A. Al-Horani, S. Kar, Potential anti-SARS-CoV-2 therapeutics that target the post-entry stages of the viral life cycle: a comprehensive, Viruses (2020) 12.

[26] C. Amici, A. Di Caro, A. Ciucci, L. Chioppa, C. Castilletti, V. Martella, N. Decaro, C. Buonavoglia, M.R. Capobianchi, M.G. Santoro, Indomethacin has a potent antiviral activity against SARS coronavirus, Antivir Ther 11 (2006) 1021–1030.

[27] https://clinicaltrials.gov/ct2/history/NCT04344457?V_1=View.

[28] P. Kiani, A. Scholey, T.A. Dahl, L. McMann, J.M. Iversen, J.C. Verster, In vitro assessment of the antiviral activity of ketotifen, indomethacin and naproxen, alone and in combination, against SARS-CoV-2, Viruses (2021) 13.

[29] D.E. Gordon, J. Hiatt, M. Bouhaddou, V.V. Rezelj, S. Ulferts, H. Braberg, A.S. Jureka, K. Obernier, J.Z. Guo, J. Batra, R.M. Kaake, A.R. Weckstein, T.W. Owens, M. Gupta, S. Pourmal, E.W. Titus, M. Cakir, M. Soucheray, M. McGregor, Z. Cakir, G. Jang, M.J. O'Meara, T.A. Tummino, Z. Zhang, H. Foussard, A. Rojc, Y. Zhou, D. Kuchenov, R. Huttenhain, J. Xu, M. Eckhardt, D.L. Swaney, J.M. Fabius, M. Ummadi, B. Tutuncuoglu, U. Rathore, M. Modak, P. Haas, K.M. Haas, Z.Z.C. Naing, E.H. Pulido, Y. Shi, I. Barrio-Hernandez, D. Memon, E. Petsalaki, A. Dunham, M.C. Marrero, D. Burke, C. Koh, T. Vallet, J.A. Silvas, C.M. Azumaya, C. Billesbolle, A.F. Brilot, M.G. Campbell, A. Diallo, M.S. Dickinson, D. Diwanji, N. Herrera, N. Hoppe, H.T. Kratochvil, Y. Liu, G.E. Merz, M. Moritz, H.C. Nguyen, C. Nowotny, C. Puchades, A.N. Rizo, U. Schulze-Gahmen, A.M. Smith, M. Sun, I.D. Young, J. Zhao, D. Asarnow, J. Biel, A. Bowen, J.R. Braxton, J. Chen, C.M. Chio, U.S. Chio, I. Deshpande, L. Doan, B. Faust, S. Flores, M. Jin, K. Kim, V.L. Lam, F. Li, J. Li, Y.L. Li, Y. Li, X. Liu, M. Lo, K.E. Lopez, A.A. Melo, F.R. Moss 3rd, P. Nguyen, J. Paulino, K.I. Pawar, J.K. Peters, T.H. Pospiech Jr., M. Safari, S. Sangwan, K. Schaefer, P.V. Thomas, A.C. Thwin, R. Trenker, E. Tse, T.K.M. Tsui, F. Wang, N. Whitis, Z. Yu, K. Zhang, Y. Zhang, F. Zhou, D. Saltzberg, Q.S.B. Consortium, A.J. Hodder, A.S. Shun-Shion, D.M. Williams, K.M. White, R. Rosales, T. Kehrer, L. Miorin, E. Moreno, A.H. Patel, S. Rihn, M.M. Khalid, A. Vallejo-Gracia, P. Fozouni, b C.R. Simoneau, T.L. Roth, D. Wu, M.A. Karim, M. Ghoussaini, I. Dunham, F. Berardi, S. Weigang, M. Chazal, J. Park, J. Logue, M. McGrath, S. Weston, R. Haupt, C.J. Hastie, M. Elliott, F. Brown, K.A. Burness, E. Reid, M. Dorward, C. Johnson, S.G. Wilkinson, A. Geyer, D.M. Giesel, C. Baillie, S. Raggett, H. Leech, R. Toth, N. Goodman, K.C. Keough, A.L. Lind, C. Zoonomia, R.J. Klesh, K.R. Hemphill, J. Carlson-Stevermer, J. Oki, K. Holden, T. Maures, K.S. Pollard, A. Sali, D.A. Agard, Y. Cheng, J.S. Fraser, A. Frost, N. Jura, T. Kortemme, A. Manglik, D.R. Southworth, R.M. Stroud, D.R. Alessi, P. Davies, M.B. Frieman, T. Ideker, C. Abate, N. Jouvenet, G. Kochs, B. Shoichet, M. Ott, M. Palmarini, K.M. Shokat, A. Garcia-Sastre, J.A. Rassen, R. Grosse, O.S. Rosenberg, K.A. Verba, C.F. Basler, M. Vignuzzi, A.A. Peden, P. Beltrao, N.J. Krogan, Comparative host-coronavirus protein interaction networks reveal pan-viral disease mechanisms, Science 370 (2020).

[30] R. Terracciano, M. Preiano, A. Fregola, C. Pelaia, T. Montalcini, R. Savino, Mapping the SARS-CoV-2-host protein-protein interactome by affinity purification mass spectrometry and proximity-dependent biotin labeling: a rational and straightforward route to discover host-directed anti-SARS-CoV-2 therapeutics, International journal of molecular sciences 22 (2021).

[31] J.R. Vane, Inhibition of prostaglandin synthesis as a mechanism of action for aspirin-like drugs, Nature: New biology 231 (1971) 232–235.

[32] P. Martin-Acosta, X. Xiao, PROTACs to address the challenges facing small molecule inhibitors, European journal of medicinal chemistry 210 (2021) 112993.

[33] L.M. Luh, U. Scheib, K. Juenemann, L. Wortmann, M. Brands, P.M. Cromm, Prey for the proteasome: targeted protein degradation-A medicinal chemist's perspective, Angewandte Chemie 59 (2020) 15448–15466.
[34] D.A. Nalawansha, C.M. Crews, PROTACs: an emerging therapeutic modality in precision medicine, Cell chemical biology 27 (2020) 998–1014.
[35] G.M. Burslem, C.M. Crews, Proteolysis-targeting chimeras as therapeutics and tools for biological discovery, Cell 181 (2020) 102–114.
[36] M. Pettersson, C.M. Crews, PROteolysis TArgeting Chimeras (PROTACs) - past, present and future, Drug discovery today. Technologies 31 (2019) 15–27.
[37] M.J. Bond, C.M. Crews, Proteolysis targeting chimeras (PROTACs) come of age: entering the third decade of targeted protein degradation, RSC chemical biology 2 (2021) 725–742.
[38] S.L. Paiva, C.M. Crews, Targeted protein degradation: elements of PROTAC design, Current opinion in chemical biology 50 (2019) 111–119.
[39] B.E. Smith, S.L. Wang, S. Jaime-Figueroa, A. Harbin, J. Wang, B.D. Hamman, C.M. Crews, Differential PROTAC substrate specificity dictated by orientation of recruited E3 ligase, Nature communications 10 (2019) 131.
[40] D.P. Bondeson, B.E. Smith, G.M. Burslem, A.D. Buhimschi, J. Hines, S. Jaime-Figueroa, J. Wang, B.D. Hamman, A. Ishchenko, C.M. Crews, Lessons in PROTAC design from selective degradation with a promiscuous warhead, Cell chemical biology 25 (2018) 78–87, e75.
[41] M. de Wispelaere, G. Du, K.A. Donovan, T. Zhang, N.A. Eleuteri, J.C. Yuan, J. Kalabathula, R.P. Nowak, E.S. Fischer, N.S. Gray, P.L. Yang, Small molecule degraders of the hepatitis C virus protease reduce susceptibility to resistance mutations, Nature communications 10 (2019) 3468.
[42] Y. Liu, C. Liang, L. Xin, X. Ren, L. Tian, X. Ju, H. Li, Y. Wang, Q. Zhao, H. Liu, W. Cao, X. Xie, D. Zhang, Y. Wang, Y. Jian, The development of Coronavirus 3C-Like protease (3CL(pro)) inhibitors from 2010 to 2020, European journal of medicinal chemistry 206 (2020) 112711.
[43] K. Raina, J. Lu, Y. Qian, M. Altieri, D. Gordon, A.M. Rossi, J. Wang, X. Chen, H. Dong, K. Siu, J.D. Winkler, A.P. Crew, C.M. Crews, K.G. Coleman, PROTAC-induced BET protein degradation as a therapy for castration-resistant prostate cancer, Proc Natl Acad Sci U S A 113 (2016) 7124–7129.
[44] J. Desantis, R.J. Vaz, US, in: Bi-functional Compounds and Methods for Targeted Ubiquitination of Androgen Receptor, 2020, 20200282068. Sep. 10.
[45] A. Simonis, S.J. Theobald, G. Fatkenheuer, J. Rybniker, J.J. Malin, A comparative analysis of remdesivir and other repurposed antivirals against SARS-CoV-2, EMBO molecular medicine 13 (2021), e13105.
[46] E. Carosati, S. Sciabola, G. Cruciani, Hydrogen bonding interactions of covalently bonded fluorine atoms: from crystallographic data to a new angular function in the GRID force field, J Med Chem 47 (2004) 5114–5125.
[47] P.J. Goodford, A computational procedure for determining energetically favorable binding sites on biologically important macromolecules, J Med Chem 28 (1985) 849–857.
[48] K. Lin, P. Gallay, Curing a viral infection by targeting the host: the example of cyclophilin inhibitors, Antiviral research 99 (2013) 68–77.
[49] M. Tampere, A. Pettke, C. Salata, O. Wallner, T. Koolmeister, A. Cazares-Korner, T. Visnes, M.C. Hesselman, E. Kunold, E. Wiita, C. Kalderen, M. Lightowler, A.S. Jemth, J. Lehtio, A. Rosenquist, U. Warpman-Berglund, T. Helleday, A. Mirazimi, R. Jafari, M.R. Puumalainen, Novel broad-spectrum antiviral inhibitors targeting host factors essential for replication of pathogenic RNA viruses, Viruses (2020) 12.
[50] A. Loregian, D.M. Coen, Selective anti-cytomegalovirus compounds discovered by screening for inhibitors of subunit interactions of the viral polymerase, Chemistry & biology 13 (2006) 191–200.
[51] H.M. Berman, J. Westbrook, Z. Feng, G. Gilliland, T.N. Bhat, H. Weissig, I.N. Shindyalov, P.E. Bourne, The protein Data Bank, Nucleic acids research 28 (2000) 235–242.
[52] S. Bienert, A. Waterhouse, T.A. de Beer, G. Tauriello, G. Studer, L. Bordoli, T. Schwede, The SWISS-MODEL Repository-new features and functionality, Nucleic acids research 45 (2017) D313–D319.
[53] https://www.uniprot.org/uniprot/Q9H7Z7.
[54] T. Yamada, F. Takusagawa, PGH2 degradation pathway catalyzed by GSH-heme complex bound microsomal prostaglandin E2 synthase type 2: the first example of a dual-function enzyme, Biochemistry 46 (2007) 8414–8424.
[55] M.S. Gadd, A. Testa, X. Lucas, K.H. Chan, W. Chen, D.J. Lamont, M. Zengerle, A. Ciulli, Structural basis of PROTAC cooperative recognition for selective protein degradation, Nature chemical biology 13 (2017) 514–521.
[56] https://www.moldiscovery.com/software/grid.
[57] J.S. Mason, A. Bortolato, D.R. Weiss, F. Deflorian, B. Tehan, F.H. Marshall, High end GPCR design: crafted ligand design and druggability analysis using protein structure, lipophilic hotspots and explicit water networks, In Silico Pharmacol 1 (2013) 23.